frontiers | Frontiers in Soft Matter

TYPE Original Research
PUBLISHED 15 September 2022
DOI 10.3389/frsfm.2022.973821

OPEN ACCESS

EDITED BY
Kay Saalwächter,
Martin-Luther-University Halle-Wittenberg, Germany

REVIEWED BY
Quan Chen,
Changchun Institute of Applied Chemistry (CAS), China
Andrij Pich,
RWTH Aachen University, Germany

*CORRESPONDENCE
Martin D. Hager,
martin.hager@uni-jena.de
Ulrich S. Schubert,
ulrich.schubert@uni-jena.de

SPECIALTY SECTION
This article was submitted to Polymers, a section of the journal Frontiers in Soft Matter

RECEIVED 20 June 2022
ACCEPTED 17 August 2022
PUBLISHED 15 September 2022

CITATION
Kampes R, Meurer J, Hniopek J, Bernt C, Zechel S, Schmitt M, Popp J, Hager MD and Schubert US (2022), Exploring the principles of self-healing polymers based on halogen bond interactions. *Front. Soft. Matter* 2:973821. doi: 10.3389/frsfm.2022.973821

Exploring the principles of self-healing polymers based on halogen bond interactions

Robin Kampes[1,2], Josefine Meurer[1,2], Julian Hniopek[2,3,4], Carolin Bernt[1,2], Stefan Zechel[1,2], Michael Schmitt[3,5], Jürgen Popp[2,3,4,5], Martin D. Hager[1,2]* and Ulrich S. Schubert[1,2,5]*

[1]Laboratory of Organic and Macromolecular Chemistry (IOMC), Friedrich Schiller University Jena, Jena, Germany, [2]Jena Center for Soft Matter (JCSM), Friedrich Schiller University Jena, Jena, Germany, [3]Institute of Physical Chemistry (IPC), Friedrich Schiller University Jena, Jena, Germany, [4]Leibniz Institute of Photonic Technology, Friedrich Schiller University Jena, Jena, Germany, [5]Abbe Center of Photonics, Friedrich Schiller University Jena, Jena, Germany

In this study, novel self-healing polymers based on halogen bonds as reversible supramolecular crosslinking moieties are presented. The reversible crosslinking is facilitated by a polymer-bound bidentate halogen bond donor entity in combination with small molecule acceptor suberic acid. The binding strength of the crosslinking can be tuned *via* deprotonation of the diacid crosslinker. The material characteristics are investigated with several methods such as NMR and Raman spectroscopy, thermogravimetric analysis and differential scanning calorimetry as well as rheology. The tactile profile measurements have been utilized to monitor the scratch healing ability of the polymer networks revealing excellent healing efficiencies up to 99% within 2 h at a temperature of 100°C. Thus, the self-healing ability of halogen bond polymers could be quantified for the first time.

KEYWORDS

self-healing polymers, halogen bonds, stimuli-responsive polymers, supramolecular polymers, crosslinked polymers

1 Introduction

The increasing demand for different polymeric materials comes with a huge consumption of resources, in particular, the petrochemical feedstock. However, these resources are limited and their consumption goes in hand with significant environmental impact, such as high carbon dioxide emissions as well as the ever growing plastics waste. (Shen et al., 2020) To increase the lifespans of products and, hence, to reduce the demand for costly and polluting replacement of used/damaged materials, the development of self-healing materials is an important research topic. (Hager et al., 2010) Self-healing polymers can in general be divided into extrinsic and intrinsic self-healing materials. While the former polymers require an encapsulated healing agent, which is usually embedded into the polymer matrix (White et al., 2001), the latter materials are able to heal a damage on their own. (Garcia, 2014) A common way to achieve this capability is the implementation

of reversible bonds into a polymer network. (Dahlke et al., 2018a) The activation of these reversible bonds, either covalent or supramolecular in nature, creates a mobile phase, which is required for the healing of the damage (*e.g.*, closure of a crack). Besides reversible covalent bonds (Bose et al., 2014; Zechel et al., 2017) several supramolecular interactions like hydrogen bonds (HB) (Cordier et al., 2008; Chen et al., 2012), ionic interactions (Han et al., 2007; Varley et al., 2010), metal-ligand complexes (Burnworth et al., 2011; Bode et al., 2013), host-guest interactions (Zhang et al., 2012) and halogen bonds (XB) (Tepper et al., 2017; Dahlke et al., 2018b) can also facilitate the reversible crosslinking. (Enke et al., 2016).

The latter is by definition the interaction between a XB donor (*i.e.* Lewis acid) and a XB acceptor (*i.e.* Lewis base). (Desiraju Gautam et al., 2013; Gilday et al., 2015; Cavallo et al., 2016) The halogen atom X, covalently bound to a polarizing group R, forms the XB donor R–X. The polarization of X results in the formation of a Lewis acidic region on the surface of the halogen atom, the so called σ-hole. (Clark et al., 2007) XBs play an emerging role in anion recognition chemistry (Robinson et al., 2015; Pancholi and Beer, 2020), crystal engineering (Mukherjee et al., 2014; Teyssandier et al., 2020) or organo-catalysis. (Bulfield and Huber, 2016; Sutar and Huber, 2019) A rather new field for XBs are supramolecular-driven smart polymer materials. (Vanderkooy and Taylor, 2015; Kampes et al., 2021; Meurer et al., 2022) Despite their analogies to HB-based materials, there are only very few reports on designing such materials. Hereby two different approaches have been utilized for the preparation of self-healing XB-based polymers. (Tepper et al., 2017; Dahlke et al., 2018b) Firstly, a XB-crosslinked material was obtained by the combination of a XB donor polymer with a complementary XB acceptor polymer. (Tepper et al., 2017) Secondly, the XB crosslinking of an ionomer with a bifunctional XB donor motif was performed. (Dahlke et al., 2018b) In both cases, the XB-based materials revealed advantageous properties compared to structurally analog HB-based or ionic materials in terms like scratch healing or hardness of the material. However, currently only one XB donor motif could be utilized successfully and the investigation of the dependency of the structure on the healing behavior was not possible. For this purpose, a detailed study and a quantification of the healing performance of such supramolecular polymers is required.

Consequently, we were aiming to further develop the strategy of using XB-interactions in this study. In order to investigate the structural influence on the healing behavior, we changed the XB donor moiety resulting in a weaker supramolecular interaction compared to our previous literature reports. (Tepper et al., 2017; Dahlke et al., 2018b) Hence, we synthesized a XB donor polymer, which could be crosslinked with a dicarboxylic acid as bifunctional XB acceptor. Neutralization of this crosslinker allows a tuning of the binding strength. In order to study the healing process in detail, tactile profile measurements were utilized. Thus, a quantification of the self-healing ability at different times and temperatures was possible providing more insights into the crack closure ability of XB-based supramolecular polymers.

2 Results and discussion

2.1 Synthesis of XB-polymers

To synthesize reversible supramolecular crosslinked polymers *via* XB, it was required to synthesize a polymer bearing the XB donor moieties in its side chains. For this purpose, **XB-MA**, a methacrylamide-based monomer featuring a XB donor, was prepared according to the literature. (Meurer et al., 2022) Subsequently, the XB donor polymer (**P1**) was synthesized *via* reversible addition-fragmentation chain-transfer (RAFT) polymerization of the monomer XB-MA and butyl methacrylate (BMA) as comonomer (Scheme 1a). A monomer ratio of BMA to **XB-MA** of 20:1 was utilized for the polymerization to guarantee a suitable degree of crosslinking. The resulting polymer was characterized *via* size exclusion chromatography (SEC) and elemental analysis (EA). The exact composition of **P1** was calculated *via* ^{1}H NMR spectroscopy. A comparison between the BMA O-CH_2 integral and the aromatic mesityl hydrogens of the **XB-MA** unit (4H) revealed a 31 to 1 ratio of BMA to **XB-MA** in the polymer **P1** (Supplementary Information, Supplementary Figure S4) indicating a slightly lower content of XB donor moieties compared to the ratio used for the polymerization. This content could further be confirmed *via* the determined iodine content in the elemental analysis. The SEC investigation revealed a molar mass of 11,600 g mol^{-1} (M_n), respectively 13,500 g mol^{-1} (M_w) and a low dispersity (Đ = 1.17) typical for RAFT-polymerizations.

Subsequently, the supramolecular crosslinked polymer network (**P2**) was synthesized (see Scheme 1b). For this purpose, a solution of the polymer **P1** was simply mixed with a solution of suberic acid (both diluted in tetrahydrofuran (THF)). Evaporating the solvent resulted in the formation of **P2**. The optimal ratio of the *bis*-carbonic acid was estimated using the content of halogen donor units in **P1** aiming for 0.5 equivalents of the bifunctional crosslinker. In order to increase the strength of the supramolecular crosslinking, the conversion of the carboxylic acids to their corresponding anions was performed. For different XB systems the conversion to the ionic species leads to an increase by orders of magnitude.

For this purpose, **P2** was treated with tetrabutylammonium hydroxide (TBAOH) solution to obtain the dicarboxylate. For that, solutions of **P2** and TBAOH in respect to the linker content of **P2** were mixed, followed by evaporation resulting in the formation of **P3**. The synthesis of **P3** is also schematically displayed in Scheme 1c.

The polymers **P2** and **P3** were investigated using ^{1}H NMR spectroscopy and elemental analysis as well. While the linker's signals are mostly covered by the polymer backbone, TBA was

found in the ^{1}H NMR spectrum of **P3**. However, the occurrence of XBs in solution at the measured conditions is only indicated by a very small shift of the signals corresponding to the carbazole's protons due to the very weak interaction and hence, less influence of the supramolecular bond formation on the aromatic hydrogen atoms can be observed. Therefore, the XB was investigated in the solid state with temperature dependent Raman spectroscopy and rheology as reported in the following paragraphs.

2.2 Polymer characterization

2.2.1 Thermal properties

We investigated the thermal properties of polymers **P1**, **P2** and **P3** with thermogravimetric analysis (TGA) and differential scanning calorimetry (DSC) (see Table 1), in order to understand later the ability for self-healing. The degradation temperature (T_d) was investigated *via* TGA defined as 95% remaining mass (see Supplementary Figure S6) and degradation temperatures above 220°C for **P1** and **P2** were found. In contrast, for the sample **P3**, a lower T_d-value of 191°C was determined. The T_d decrease presumably results from the tetra-butyl ammonium counterion, which remains after the neutralization step in the ionic polymer **P3**. This behavior could already be observed in other studies, in which this counter ion was utilized in other polymeric materials. (Meurer et al., 2021) Nevertheless, the TGA investigations for all samples revealed hight thermal stabilites enabeling thermal induced self-healing experiments without a decomposition of the polymers. Furthermore, the glass transition temperatures were determined with dynamic scanning calorimetry (see Supplementary Figure S7 and Supplementary Table S1). All polymers revealed T_g-values around 30°C, showing a rather small influence of the supramolecular crosslinking on the

TABLE 1 Determined degradation and glass transition temperatures of the polymers P1 to P3 *via* TGA and DSC.

Polymer	P1	P2	P3
T_d [°C]	250	224	191
T_g [°C]	31	33	34

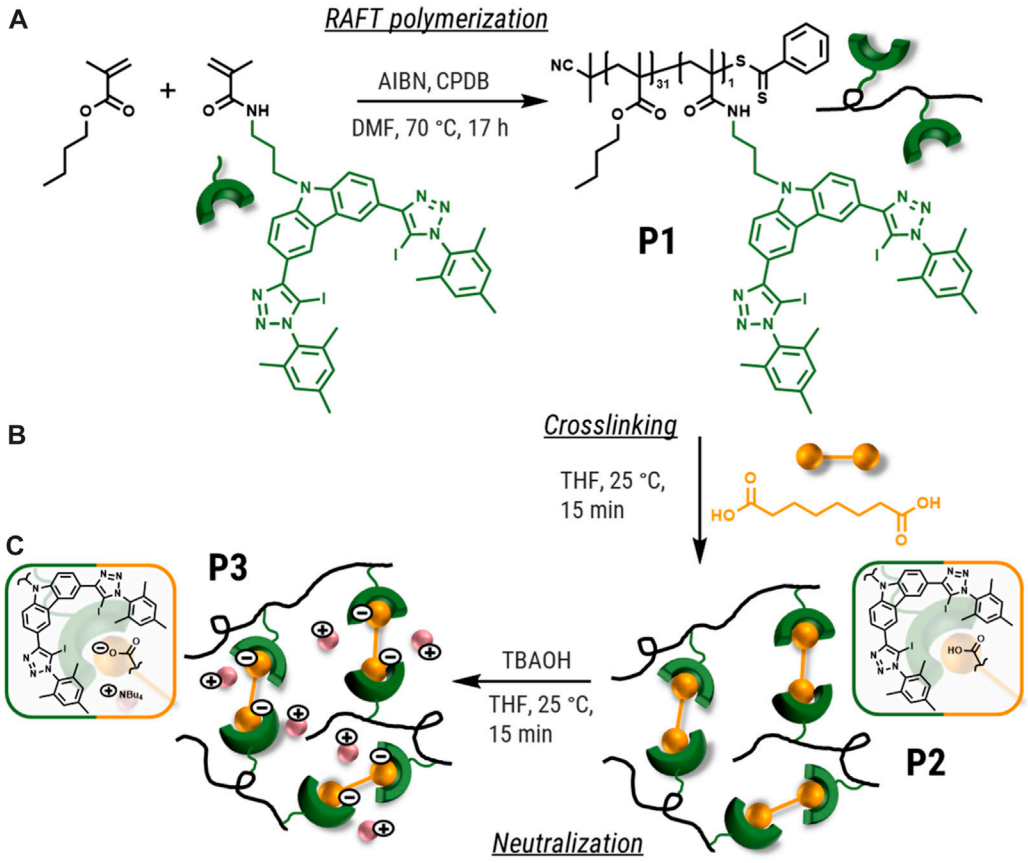

SCHEME 1
Schematic representation of the synthesis of the polymers **P1** (a—RAFT polymerization), **P2** (b—crosslinking) and **P3** (c—neutralization).

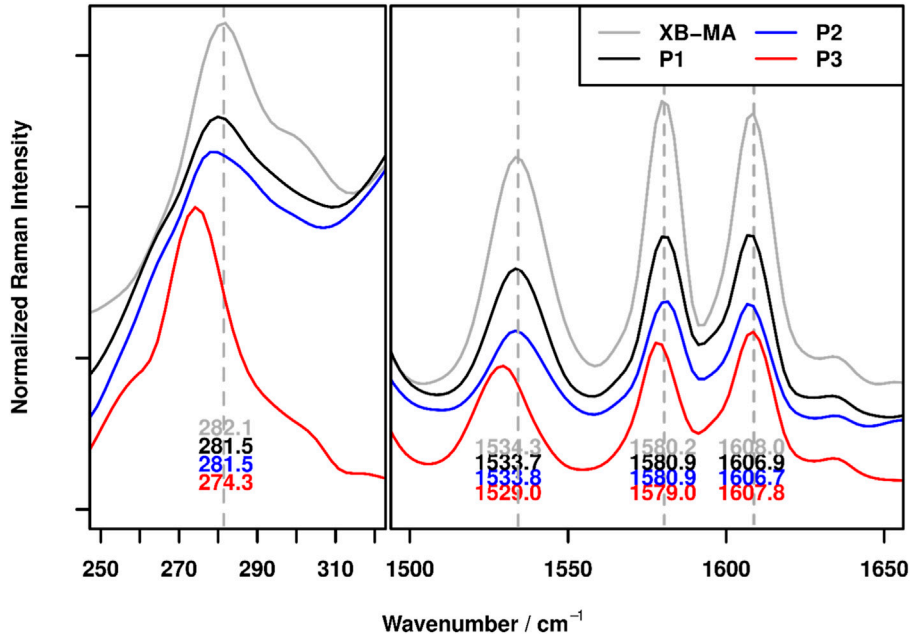

FIGURE 1
FT-Raman spectra of **XB-MA** and the polymers **P1** (non-crosslinked), **P2** (acid crosslinked) and **P3** (neutralized crosslinked) in the wavenumber regions characteristic for XBs. In order to visualize the band shift, grey dotted lines, corresponding to the pea maxima of **XB-MA** were added to figure.

thermal properties. Nevertheless, small differences of the glass transition temperatures between **P1** to **P3** were found. The determined values increase from **P1** to **P2**, presumably caused by the formation of the supramolecular crosslinking. Furthermore, the neutralization of the carboxylic groups increases the glass transition temperature slightly due to the stronger XB interaction in **P3**.

2.2.2 Raman spectroscopic investigation

To confirm the presence of XB in the supramolecular crosslinked polymers **P2** to **P3**, Raman spectroscopy was performed for the samples **P1** to **P3** as well as the monomer **XB-MA** containing the XB donor moiety. As a spectroscopic method with molecular specificity, Raman spectroscopy is well suited to investigate the binding conditions within complex polymer environments and is able to directly observe the presence of the supramolecular bonding. (Messina et al., 2000; Wang et al., 2019) It has successfully been applied in the past to investigate specifically XB in self-healing (Tepper et al., 2017; Dahlke et al., 2018b) as well as in shape-memory polymers. (Meurer et al., 2022)

Based on earlier investigation of the **XB-MA** donor (Meurer et al., 2022), characteristic Raman bands (ca. 282 cm^{-1} (ν(C-X)) and 1,534, 1,580, 1,608 cm^{-1} (ν(C-C/N_{ar})) could be identified, which shift in position upon binding to a XB acceptor. The shift is caused by the population of σ*(C-X) orbitals (Messina et al., 2000; Rosokha et al., 2013; Wang et al., 2019), which leads to a lengthening of the C-X bond and changes the electron density in the triazole moieties of **XB-MA**.

Figure 1 depicts the relevant wavenumber regions for the free **XB-MA** donor as well as the non-crosslinked polymer P1 and the crosslinked polymers **P2** (carboxylic acid) and **P3** (neutralized). First, it can be seen that the incorporation of **XB-MA** into the polymer **P1** only has very minimal effect on the respective band positions indicating that its structure is generally maintained. The small shifts can be attributed to electrostatic influences of the polymer environment, which cause small differences in band positions similar to the well-known changes of band positions upon dissolution of samples in a solvent. (Socrates, 2001) Second, the characteristic shifts of the C-X vibration at 282 cm^{-1} by roughly 8 cm^{-1} to 274 cm^{-1} as well as the changes to the C-C/N_{ar} vibrations can clearly be identified for the neutralized polymer **P3** proving the presence of XB within this polymer.

For the polymer **P2**, containing carboxylic acid, no significant shifts in band positions could be observed compared to the non-crosslinked polymer **P1**. While this makes it impossible to definitely confirm the presence of XBs within the polymer, this observation is in line with previous results on XB-based polymers. (Meurer et al., 2022) Since XBs formed with free carboxylic acids are much weaker compared to ionic species (Lieffrig et al., 2013), less changes to the electronic structure and, thus, the vibrational structure are expected. While in previous works, a small shift of ca. 1 cm^{-1} for the C-X vibration could be observed for these kinds of XB, this could just be an

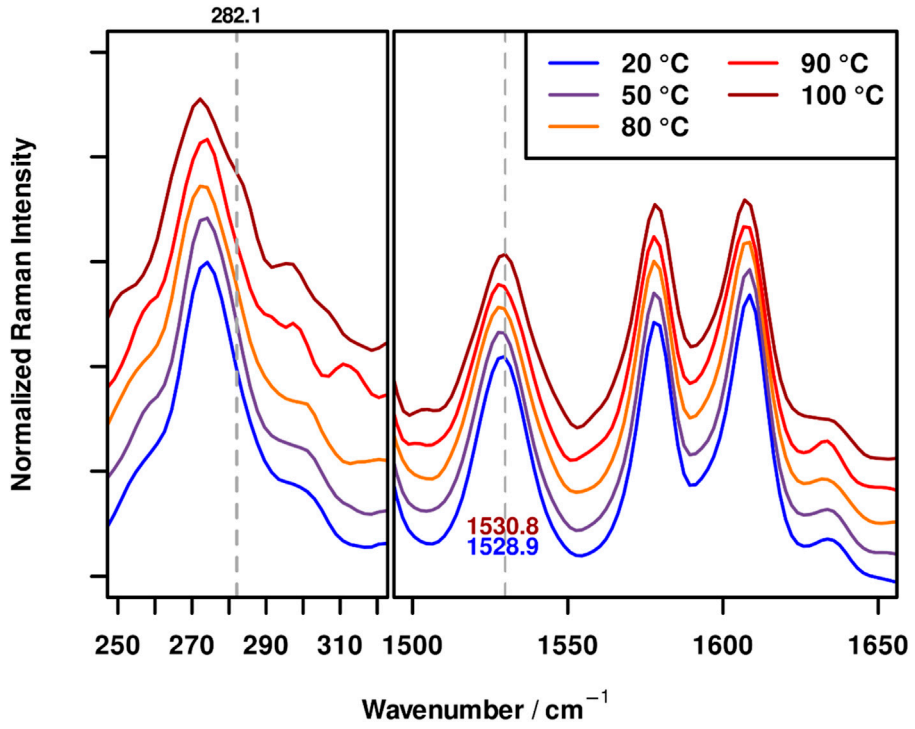

FIGURE 2
FT-Raman spectra of **P3** at 20 (blue), 50 (violet), 80 (orange), 90 (red) and 100°C (dark red) in the wavenumber regions characteristic for XBs. In order to visualize the band shifts, grey dotted lines, corresponding to the peak maxima of the spectra at 100°C were added to figure.

indication of a slightly weaker XB, thereby moving the shift beyond the resolution capabilities of the Raman instrumentation. The very weak interaction on the other hand is a very promising finding for the self-healing behavior, since weaker crosslinking should result in better healing abilities.

To further confirm that the XB is responsible for the self-healing behavior of the polymer, a temperature dependent Raman experiment was carried out for **P3** by heating the sample from ambient temperature to 100°C in 10 K steps and recording a Raman spectrum at each temperature. Figure 2 depicts the resulting Raman spectra for selected temperatures.

It can be seen that the Raman spectrum of **P3** remains completely unaffected up to 90°C. Thus, no changes in the X-bond sensitive wavenumber regions could be observed. At 90°C a very small shift of the band maximum of the ν(C-I) bond at 274 cm^{-1} to higher wavenumbers and slight broadening can be seen; however, it is still in the range of the spectral precision of the instrument (ca 0.5 cm^{-1}). For the measurement at 100°C on the other hand, the appearance of a shoulder at 282 cm^{-1}, coinciding with the position of the ν(C-I) in the free **XB-MA** is clearly visible. This shoulder is accompanied by a shift of the aromatic band at ca. 1,529 cm^{-1} by roughly 2 cm^{-1} to higher wavenumbers. These changes clearly indicate the presence of unbound XB donor moieties in the polymer **P3** at 100°C, as the observed changes upon complexation are (partially) reversed. Considering that slight changes can be already observed at 90°C and the fact that the heating device is an open system, thereby making a deviation of the polymer temperature compared to the heating plate plausible, these findings match well with the frequency sweep measurements (see below) and limited self-healing ability at 80°C (see below) whereas at 100°C good self-healing behavior could be observed. These results were obtained for **P3**, since the ionic nature of the supramolecular bond leads to the largest shifts in Raman bands enabling a detailed investigation of signal shifts. Nevertheless, these results can readily be transferred to **P2**, thereby corroborating the XB-based self-healing mechanism of these polymers.

2.2.3 Frequency dependent dynamic-mechanical analysis

It is possible to gain more insights into the structure of polymers and its macroscopic behavior using rheological investigations. (Lange et al., 1999; Bose et al., 2014) For instance, the reversibility of supramolecular crosslinking can be studied applying frequency dependent dynamic-mechanical analyses (DMA). (Bose et al., 2015) Consequently, frequency sweep measurements were performed with the samples **P2** and **P3** at different temperatures (see Supplementary Figures S8, S9).

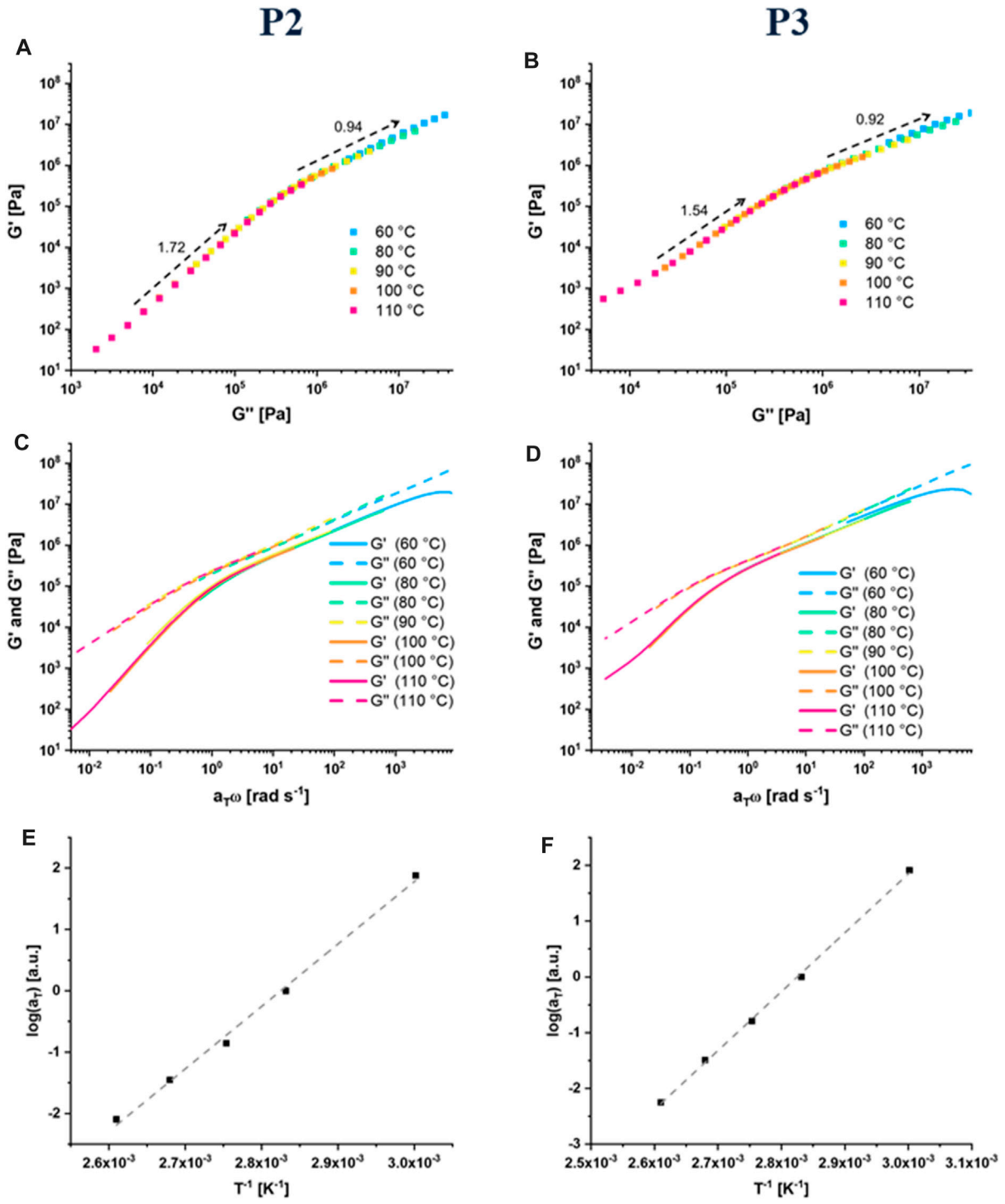

FIGURE 3
Results of the rheological investigations: logG′ to logG″ plot for **P2 (A)** and **P3 (B)**, master curves at T_{ref} = 80°C for **P2 (C)** and **P3 (D)** and Arrhenius plot of the shift factors for **P2 (E)** and **P3 (F)**.

The measurements of both samples revealed comparable results, since both polymers behave similar during the thermal treatment. At a temperature of 25°C the storage modulus (G′) is over the whole frequency range constantly higher than the loss modulus (G″) revealing a rather solid and stiff character of the sample. Raising the temperature above to the glass transition

temperature and the expected activation temperature of the supramolecular bonds leads to a change of this behavior. During the frequency dependent DMA at 100°C, G″ is higher than G' over the whole frequency range. A similar behavior has also been observed for linear poly (n-butyl acrylates), which were partially hydrolyzed resulting in the formation of hydrogen bonds. (Hawke et al., 2016).

Han *et al.* introduced logarithmic plots of the storage and loss modulus, which can reveal correlations almost independently of the temperature. (Han and Jhon, 1986) These plots have been utilized besides homopolymers also for block copolymers (Ogawa et al., 1996) or polymer blends. (Yang and Han, 2008) Based on these findings, the logarithmic plots of G′ vs. G`` at different temperatures and frequencies can be found in Figures 3A,B). For both polymers, the curves indicate a temperature dependent structural change, since the slope increases with the temperature from 0.9 (60–80°C) to 1.7 for **P2** and 1.5 in case of **P3** (90–110°C), respectively. Therefore, it seems, that with increasing temperature the determined slope in the lower frequency range keeps getting closer to the value of 2, which would represent the ideal behavior for linear non-crosslinked polymer featuring no additional interactions. (Han and Jhon, 1986; Yang and Han, 2008) For this reason, the determined behavior at the higher temperatures fits to an activation of the halogen bonds, which was also observed in the Raman measurements also indicating an opening of the halogen bonds at and above 90°C. Since the value of 2 is not completely reached, it seems that not all supramolecular crosslinking points are activated and/or opened at this temperature, which also corresponds with the Raman experiments, where signals corresponding to crosslinked moieties were still detected. Hereby, the effect is more pronounced for the polymer crosslinked with the neutralized crosslinker.

These plots also indicate that a time-temperature superposition (TTS) should be applicable. For supramolecular polymers, TTS it not always usable. (Seiffert and Sprakel, 2012) The measurements from 60 to 110°C were utilized to create the master curves for **P2** and **P3** (see Figures 3C,D) at a reference temperature (T_{ref}) of 80°C, based on the TTS analogously to literature. (Soman and Evans, 2021) For the creation of the master curves, the shifting was only performed in horizontal direction (shift factors: a_T). Even without the shifting in the vertical direction (shift factors: b_T) the curves of G′ and G″ fit extremely well, indicating a non-complex structure of the studied polymer networks. This behavior can be explained by the rather low content of supramolecular crosslinking of **P2** and **P3**. Both master curves show a reasonably good fit between all measurements. The resulting shift factors (a_T), follow an Arrhenius-type behavior (see Figures 3E,F).

This behavior has also been observed for other supramolecular polymers, whereas in some cases also a Williams–Landel–Ferry (WLF) function has been utilized for the TTS. (Seiffert and Sprakel, 2012) The measured parameters were further utilized to calculate according to literature the activation energies (E_A). (Lewis et al., 2014; Hawke et al., 2016) It was found, that both activation energies with 84.67 kJ mol^{-1} for **P2** and 87.90 kJ mol^{-1} in case of **P3**, are relative comparable, but it indicates that the activation of the "stronger crosslinked" **P3** requires a little more energy. These values are lower compared to polyacrylates crosslinked by the hydrogen bonding unit upy (ca. 120 kJ/mol). (Shabbir et al., 2016).

The results of the rheological investigations fit very well to the results of the temperature dependent FT-Raman measurements of **P3**, which indicated an opening of the halogen bond at temperatures above 90°C as stated above. Thus, a temperature increase leads to the bond activation and an opening of the supramolecular junction resulting in a decrosslinking of the networks. Thus, the structural change, bond-opening, can be studied by Raman spectroscopy and can be correlated with the changing behavior of the mechanical behavior at higher temperatures.

2.2.4 Scratch healing tests

Finally, the self-healing abilities of the XB-based materials were studied. In order to investigate the samples in a detailed and comparable fashion, a formerly established method, based on tactile profile measurements, was applied. (Abend et al., 2020) In order to prepare suitable samples with a flat surface, the supramolecular crosslinked polymers (**P2** and **P3**) were pressed in a self-manufactured mold and tempered at 130°C for 1 h. After embedding the polymer specimen into epoxy resin, grinding and polishing the samples, a defined scratch was induced into the surface of the samples with an indenter. Subsequently, the volume of the scratch was determined *via* a tactile measurement by driving the smaller indenter along the profile in a 90° angle to the scratch. The samples were then heated in an oven to trigger the healing process by activating the reversible XB interactions, followed by a second profile measurement. Exemplarily, the panorama pictures and a profile before and after healing (2 h at 100°C) of **P2** are displayed in Figure 4; the scratch is almost completely healed. The calculated healing efficiencies under different healing conditions of all measurements are listed in Table 2. Further information is presented in the Supplementary Table S1 and Supplementary Figures S10–S16.

The first self-healing investigation of **P2** and **P3** was conducted at 100°C for 5 h and resulted in a complete scratch closure in both cases. Hence, the temperature was sufficient for activation of the reversible interaction and, thus, of the material. This behavior could be expected based on the temperature dependent Raman spectroscopy and rheology measurements (see above). Subsequently, the healing time was reduced to 2 h. However, in both cases these conditions still led to a nearly complete scratch healing. Only very slight differences

TABLE 2 Overview of the scratch healing tests of P2 and P3.

Sample	Scratch	Duration	Temperature	Healing efficiency [%]
P2	1	5 h	100 °C	100
	2	2 h		99
	3	1 h		85
		+1 h		97
	4	2 h	80 °C	64
P3	1	5 h	100 °C	100
	2	2 h		96
	3	1 h		32
		+1 h		56
		+1 h		71
	4	2 h	80 °C	11

were observed with a healing efficiency of 99% for **P2** and 96% for **P3**, respectively. Within the next experiment, the healing time was further decreased to 1 h. The shorter time revealed significant differences in the healing ability between **P2** and **P3**. **P2** already healed to a large extent of 85% within the first healing procedure of 1 h and complete scratch closure was achieved during a second run (additional 1 h). In contrast, **P3** showed only partial healing, even after the third healing cycle of 1 h with steps from 32% (1 h), 56% (1 + 1 h) and 71% (1 + 1 + 1 h) healing efficiency. The corresponding scratch profiles are displayed in Figure 5. Since both materials showed a good healing at 100°C within 2 h, we also investigated the scratch healing at a lower temperature of 80°C using a constant time of 2 h. In that case, a partial healing (64%) was observed for **P2**. **P3** showed only very poor healing (11%) indicating that this temperature is not sufficient to activate the stronger XB.

The difference in the self-healing behavior of the two different polymers correlates with the binding strength of the XB-interaction in solution as well as the findings of the Raman investigations presented above. The self-healing of materials is a stepwise process and can be divided in four central steps. (Hager et al., 2010) Firstly, the damage occurs (*e.g.*, crack in the surface), followed by the generation of the "mobile phase". Subsequently, the mass-transport into the damage starts and finally the material is immobilized again. Regarding the presented self-healing polymers **P2** and **P3**, both polymers differ in their chemical structure. Whereas **P2** feature halogen-bond crosslinkers of weaker nature, **P3** exhibits much stronger supramolecular

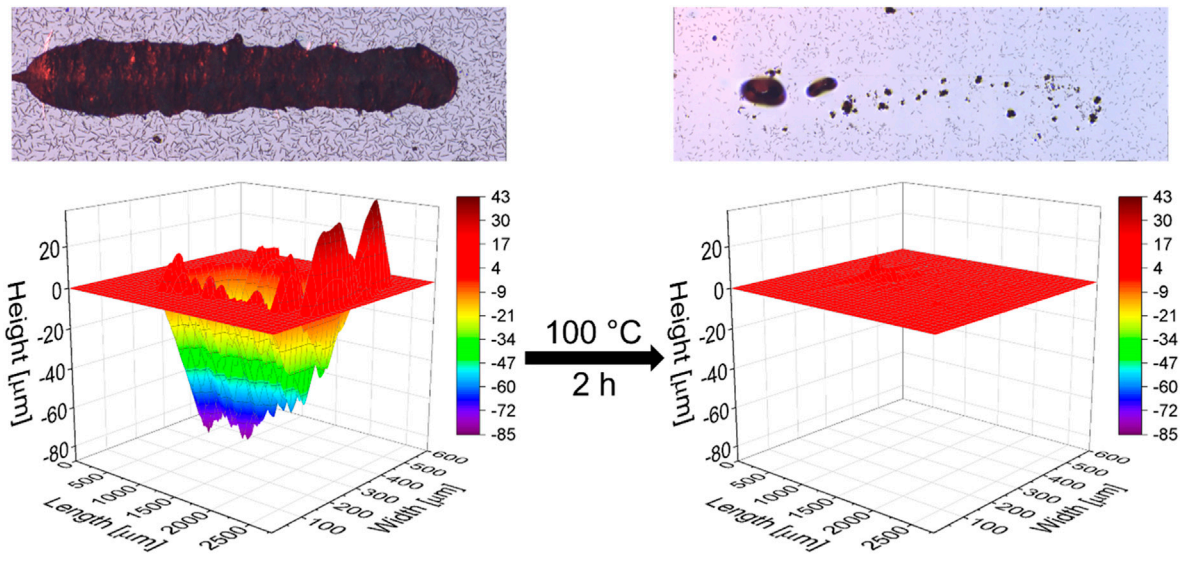

FIGURE 4
Panorama pictures (top) and profiles (bottom) before and after the scratch healing of **P2** at 100°C for 2 h.

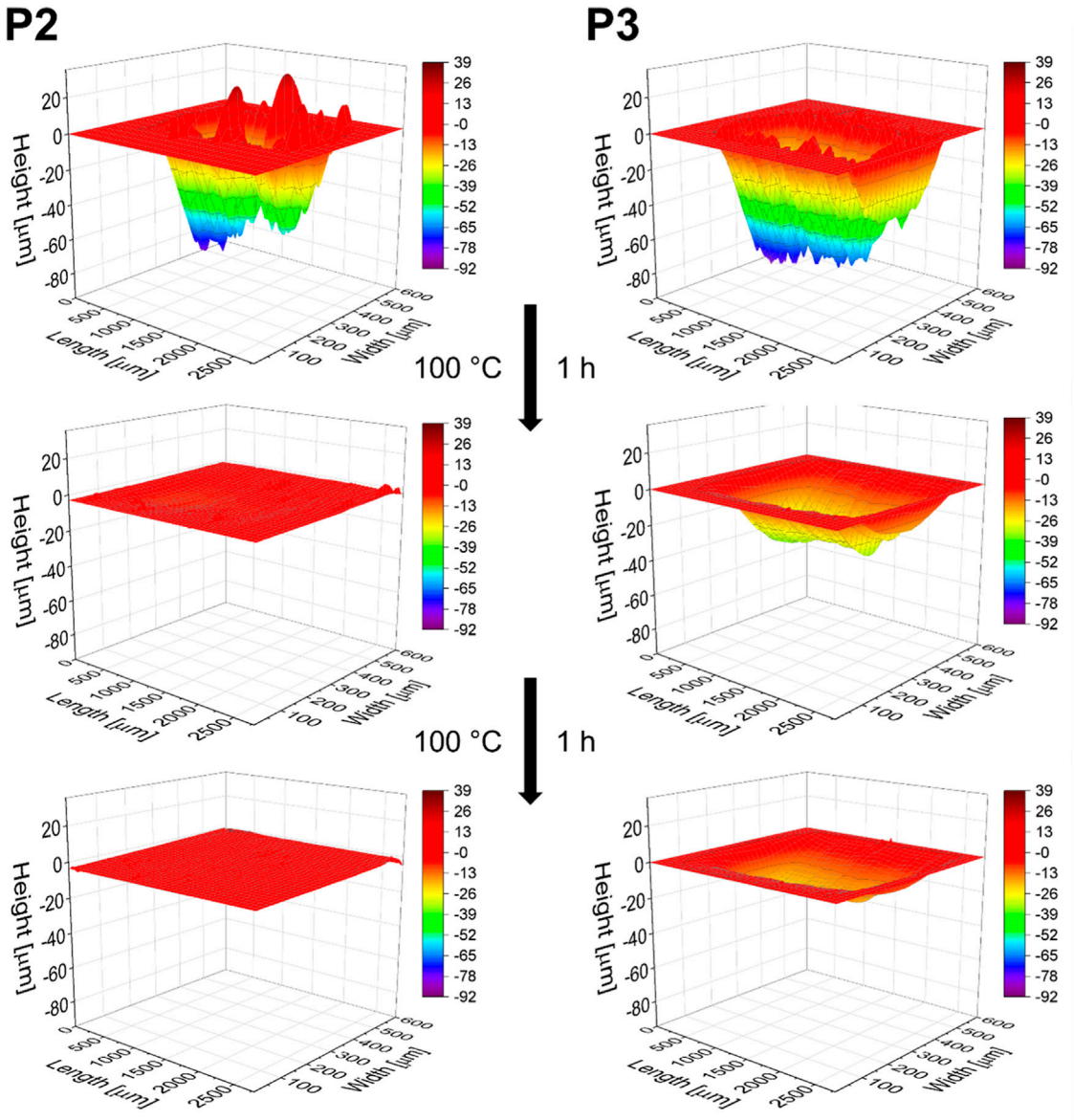

FIGURE 5
Comparison of the scratch profiles of **P2** and **P3** before and after the first and second healing step at 100°C for 1 h respectively.

crosslinks. This difference in binding strength significantly influence step 2 of the overall healing mechanism–the generation of the mobile phase. Thus, the weaker interaction of **P2** is activated even at 80°C resulting in a good healing ability at this temperature. In contrast, the strong supramolecular bond in case of **P3** is not activated at this temperature and, consequently, no healing can be observed in this case.

Hence, the finding indicates a highly reversible interaction in case of **P2** and a more stable binding in case of **P3**, which excellently correlates with the observed healing behavior.

These findings of the current study are also in line with the earlier studies regarding self-healing or shape-memory polymers based on XB-interactions. The healing ability of the polymers presented in the current study are also better compared to the XB-based materials presented previously. (Tepper et al., 2017; Dahlke et al., 2018b) In the previous studies, a stronger halogen bond motif was applied and, consequently, the healing behavior seems to strongly correlate with the binding strength of the XB. However, a detailed comparison is not possible since no quantified healing experiments were performed in the previous studies.

Nevertheless, longer healing times at 100°C could be observed in these investigations indicating an improvement within the current study.

To investigate, whether the original structure of the supramolecular crosslinked polymer network is reformed after the healing process, FT-Raman measurements were performed. Within those measurements different spectra were recorded on the surface of the samples as well as at the reformed surface after the scratch healing. This experiment was exemplarily performed for **P3**, since the characteristic signals of the halogen bond can easier be analyzed and the changes are more obvious compared to **P2**. The recorded spectra of the different areas revealed no significant differences (see Supplementary Figures S21–S23). For this reason, it is possible to conclude that the original structure of the samples is restored after the healing of the damage.

3 Conclusion

In the current study, the halogen bond could be utilized as supramolecular crosslinker for the design of self-healing materials. For this purpose, polymer **P1** was prepared featuring a bidentate XB donor entity in its side chains. Supramolecular crosslinking *via* the addition of suberic acid acting as *bis*-functional XB acceptor resulted in **P2**. The resulting XB-based crosslinking strength was afterwards increased by deprotonation of the carboxyl groups with tetrabutylammonium hydroxide resulting in **P3**. All polymers were characterized using NMR-spectroscopy, DSC, TGA and DMA measurements as well as Raman spectroscopy. The latter method could prove the formation of the halogen bonds as well as their opening at temperatures above 90°C. Both supramolecular crosslinked polymers (**P2** and **P3**) were studied in scratch healing tests utilizing a tactile measurement, which allowed a more detailed investigation compared to former studies. Both materials exhibit good self-healing ability at 100°C (H_{eff} up to 100%) even though **P2** heals slightly faster, which became more evident with shorter healing times. At 80°C this trend is more pronounced and **P3** did not notably heal, while **P2** still featured partial healing within 2 h. This finding corresponds to the expected stronger supramolecular crosslinking of **P3**, which was also indicated by Raman spectroscopy. The results of this study confirm the suitability of the halogen bond for the design of self-healing materials. For the first time, the healing of such materials could be quantified and, thus, compared in great detail. A major advantage of the XB-based polymers is that the properties of such materials can be easily tuned by the change of XB motif, *e.g.*, by increasing the binding strength due to deprotonation as shown in the current study.

4 Experimental section/methods

4.1 Materials and instrumentation

All materials used for this study were obtained from TCI Germany, Sigma Aldrich, Alfa Aesar, Fluorochem and Acros Organics. Unless otherwise stated all chemicals were used as received. BMA was destabilized over neutral aluminum oxide prior to use in the polymerizations.

^{1}H NMR spectra were recorded on a Bruker AC 300 (300 MHz) in deuterated solvents (Eurisotop) at 297 K and referenced by the solvent signals. Spectra are displayed in the Supplementary Information (Supplementary Figures S1–S3).

Size exclusion chromatography was performed with a setup consisting of a Shimadzu CBM-20A system controller, a DGU-14A degasser, a LC-20AD pump, a SIL-20AHT auto sampler, a CTO-10AC vp oven, an SPD-20A UV-detector, a RID-10A RI-detector and PSS SDV guard/1,000 Å/1,000,000 Å (5 µm particle size) columns using a chloroform, isopropanol and triethylamine eluent [94/2/4] with 1 ml min^{-1} at 40°C and a poly (methyl methacrylate) standard. The SEC trace is displayed in the Supplementary Figure S5.

TGA measurements were conducted on a Netsch TG 209 F1 instrument under nitrogen atmosphere using a heating speed of 10 K min^{-1}. DSC measurements were performed using a Netsch DSC 204 F1 Phoenix instrument with 20 K min^{-1} heating for the first two cycles and 10 K min^{-1} during the third cycle. A Vario El III instrument (Elementar) was used for CHN-analyses. The data is displayed in the Supplementary Figures S6, S7.

The self-healing samples were prepared according to literature. (Dahlke et al., 2020) The polymer samples were hot pressed at a temperature of 130°C using a weight of 2–3 t and subsequently embedded in epoxy resin made from the components Epoxy Resin L and Hardener CL (R&G Faserverbundstoffe GmbH). The surface was then grinded with sandpaper (P60 to P3000).

All self-healing experiments were conducted using an Anton Paar MST^3 instrument on a STeP 4 platform. Scratch application was performed with a 50 µm Rockwell indenter. For that purpose, the indenter was moved 2000 µm over the surface with a force of 1,500 mN and a speed of 30,000 µm s^{-1} for 15 times (one directional). Subsequently, panorama pictures were taken with the optical microscope using MPlan N 5×/0.10/FN22. The samples were rotated 90°

TABLE 3 Settings used for Raman spectroscopy of the different samples.

Sample	Power/mW	Scans	Sample	Power/mW	Scans
P1	200	1,024	**P3**	200	1,024
P2	200	1,024	**XB-MA**	100	4,096

for the profile measurement and a10 µm Rockwell indenter was moved along the scratch every 20 µm (600 µm pathlength (800 µm for **P3**, scratch 2), 5 mN force and 200 µm min^{-1}). Evaluation and visualization were conducted using a Phyton based, GUI controlled program that utilizes the data analysis libraries pandas SciPy and NumPy for linear algebra, integration and interpolation (for detailed explanation see reference 48).

Raman-spectroscopy of the powdered samples were performed on a Multispec Fourier-transform Raman-spectrometer (Bruker Corporation, Billerica, Massachusetts, United States of America) in the range between 100 and 4,000 cm^{-1} with a spectral resolution of 4 cm^{-1} and spectral precision of ca 0.1 cm^{-1}. All spectra are displayed as Supplementary Figures S17–S20. The Raman excitation light at 1,064 nm was provided by a Nd:YAG laser (Klastech DeniCAFC-LC-3/40, Dortmund, Germany). The laser power at the sample was varied between 50 and 200 mW according to the photothermal stability of the sample to ensure no burning occurred. To improve the signal-to-noise ratio the number of accumulated scans was varied accordingly. The respective data for each sample is listed in Table 3.

Raman microscopy on a solid sample of **P3** was performed using a Ondax THz Raman spectrometer excited at 808 nm coupled to a Leica DM2000 microscopy and a Kaiser RXN1 spectrometer, equipped with a holographic grating and multi-line detector. Measurements were performed via a 50x/0.55NA Objective (Leica PL Fluotar). To ensure wavelength and intensity stability of the multi-line detection setup, the spectrometer was calibrated against neon emission, respectively white light lamps. For the measurement of the healed area, 152 points along the area (25 × 150µm, step size: 3 µm/8 µm) were recorded with an integration time of 1s and 10 accumulations. For the pristine area, 64 points (120 × 160 µm, step size 15/20 µm) were recorded using the same integration times.

For the non-tempered measurements, the powdered samples were pressed into aluminum pots and placed directly in front of the lens of the spectrometer. For the temperature dependent measurements, the pot was placed inside a tailor-made brass adapter connected to the heating plate of a Linkam LTS350. The plate was placed under a 90°C gold plated mirror, connected to the optical system of the spectrometer. The plate was heated to the respective target temperature with a heating rate of 30 K/min and left to equilibrize for 2 min before recording the spectrum.

For further evaluation, the raw Raman data was preprocessed using R 4.1.3. (R Core Team, 2021) The spectra were restricted to the wavenumber of interest (200–3,200 cm^{-1}) followed by background correction using the SNIP-algorithm (iterations: 100, order: 3, smoothing window: 3) (Ryan et al., 1988), and normalized using euclidean vector norm.

To determine the shifts in wavenumber position of selected Raman bands sensitive to XB formation in the polymers, Voigt profiles were fitted to the respective spectra. To do so, a single Voigt profile was fitted to the respective wavenumber regions (268–292, 1,510 to 1,558, 1,566 to 1,593, 1,595 to 1,622 cm^{-1}) using a nonlinear least squares estimator (provided by function *nls* included in the stats package of R) based on the port algorithm. The Voigt profiles were obtained using the real part of the Faddeeva function using the package RcppFaddeeva. (Auguie et al., 2015)

4.2 Polymer synthesis

XB-MA was synthesized according to literature. (Meurer et al., 2022)

P1: 0.129 g **XB-MA** (1.41 mmol), 4.00 g BMA (28.13 mmol) and 52 mg 2-cyanopropan-2-yl benzodithioate (CPDB) (0.24 mmol) were combined in a round bottom flask. Subsequently, 9.7 mg (0.06 mmol) 2,2′-azobis (2-methylpropionitrile) (AIBN) were added *via* a stock solution in DMF, further DMF was added up to a total of 15 ml DMF (2 mol/L) and the solution was degassed with nitrogen for 50 min. Subsequently, the mixture was stirred in a preheated oil bath at 70°C for 17 h followed by evaporation of the solvent in *vacuo*. The crude product was purified *via* dialysis in tetrahydrofuran (MWCO: 3.5 kDa), while the solvent was changed two times a day for 3 days in total, and the product was dried in *vacuo* to obtain 3.41 g of an orange solid.

^{1}H NMR (300 MHz, $CDCl_3$): δ = 0.65–2.30 (m, 440H), 2.40 (s, 6H), 3.08–3.21 (m, 2H), 3.93 (s, 64H), 4.37–4.54 (m, 2H), 5.63–5.81 (m, 1H), 7.06 (s, 4H), 7.48–7.62 (m, 2H), 8.26 (d, J = 8.6 Hz), 8.92 (s, 2H) ppm.

Size exclusion chromatography (SEC) ($CHCl_3$/NEt_3/*iso*-propanol 94:4:2, PMMA standard): M_n = 11,600 g mol^{-1}; M_w = 13,500 g mol^{-1}; Đ = 1.17.

Anal. Calcd. for monomer ratio according to ^{1}H NMR: C 65.21, H 8.98, N 2.11, I 4.77; found C 65.35, H 9.06, N 1.98, I 6.44.

P2: A solution of 54 mg of suberic acid (0.31 mmol) in 5 ml tetrahydrofuran was added dropwise to a solution of 3.312 g **P1** (0.62 mmol functionality) in 20 ml tetrahydrofuran and was stirred for 1.5 h. Subsequently, the solvent was removed in *vacuo* and the product (3.36 g) was dried in *vacuo*.

^{1}H NMR (300 MHz, $CDCl_3$): δ = 0.60–2.50 (m, 651H), 3.10–3.22 (m, 2H), 3.94 (s, 93H), 4.42–4.55 (m, 2H), 5.63–5.81 (m, 1H), 7.07 (s, 4H), 7.48–7.62 (m, 2H), 8,26 (d, J = 8.6 Hz 2H), 8.92 (s, 2H) ppm.

Anal. Calcd. for monomer ratio according to ^{1}H NMR: C 65.05, H 8.96, N 2.07, I 4.69; found C 65.11, H 9.04, N 1.94, I 5.89.

P3: A solution of tetrabutylammonium hydroxide (37%, 0.078 g, 0.30 mmol) in methanol was slowly added to a solution of 1.623 g **P2** (0.15 mmol crosslinker) in tetrahydrofuran. After

10 min stirring, the solvent was removed under reduced pressure and the product (1.71 g) was dried *in vacuo*.

^{1}H-NMR (300 MHz, CDCl3): δ = 0.60–2.53 (m, 762H), 3.08–3.22 (m, 2H), 3.34 (s, 16H), 3.95 (s, 100H), 4.41–4.55 (m, 2H), 5.68–5.81 (m, 1H), 7.06 (s, 4H), 7.52–7.56 (m, 2H), 8.26 (d, J = 7.6 Hz, 2H), 8.93 (s, 2H) ppm.

Anal. Calcd. for monomer ratio according to ^{1}H NMR: C 65.67, H 9.20, N 2.23, I 4.49; found C 65.42, H 9.27, N 2.07, I 5.25.

Data availability statement

The raw data supporting the conclusion of this article can be obtained from the authors upon request.

Author contributions

Synthesis: RK, JM, and CB. Characterization: RK, JM, JH, and CB Writing—original draft: RK, JM, JH, and SZ Writing—review and editing: MS, JP, MH, and US Supervision: SZ, MS, JP, MH, and US.

Acknowledgments

The authors gratefully acknowledge Deutsche Forschungsgemeinschaft (DFG) for financial support (SCHU 1229/24-2; project number: 280016777). Furthermore, the Carl-Zeiss foundation is acknowledged for financial support (project Perspektiven 2019).

Conflict of interest

The authors declare that the research was conducted in the absence of any commercial or financial relationships that could be construed as a potential conflict of interest.

Publisher's note

All claims expressed in this article are solely those of the authors and do not necessarily represent those of their affiliated organizations, or those of the publisher, the editors and the reviewers. Any product that may be evaluated in this article, or claim that may be made by its manufacturer, is not guaranteed or endorsed by the publisher.

Supplementary material

The Supplementary Material for this article can be found online at: https://www.frontiersin.org/articles/10.3389/frsfm.2022.973821/full#supplementary-material

References

Abend, M., Tianis, L., Kunz, C., Zechel, S., Gräf, S., Müller, F. A., et al. (2020). A novel approach for the quantification of scratch healing of polymers. *Polym. Test.* 90, 106699. doi:10.1016/j.polymertesting.2020.106699

Auguie, B., Eddelbuettel, D., Johnson, S. G., and RcppFaddeeva, G.: 'Rcpp' bindings for the 'Faddeeva' package. R package version 0.1.0, https://CRAN.R-project.org/package=RcppFaddeeva, 2015.

Bode, S., Zedler, L., Schacher, F. H., Dietzek, B., Schmitt, M., Popp, J., et al. (2013). Self-healing polymer coatings based on crosslinked metallosupramolecular copolymers. *Adv. Mat.* 25, 1634–1638. doi:10.1002/adma.201203865

Bose, R. K., Hohlbein, N., Garcia, S. J., Schmidt, A. M., and van der Zwaag, S. (2015). Connecting supramolecular bond lifetime and network mobility for scratch healing in poly(butyl acrylate) ionomers containing sodium, zinc and cobalt. *Phys. Chem. Chem. Phys.* 17, 1697–1704. doi:10.1039/c4cp04015e

Bose, R. K., Kötteritzsch, J., Garcia, S. J., Hager, M. D., Schubert, U. S., and van der Zwaag, S. (2014). A rheological and spectroscopic study on the kinetics of self-healing in a single-component diels-alder copolymer and its underlying chemical reaction. *J. Polym. Sci. Part A Polym. Chem.* 52, 1669–1675. doi:10.1002/pola.27164

Bulfield, D., and Huber, S. M. (2016). Halogen bonding in organic synthesis and organocatalysis. *Chem. Eur. J.* 22, 14434–14450. doi:10.1002/chem.201601844

Burnworth, M., Tang, L., Kumpfer, J. R., Duncan, A. J., Beyer, F. L., Fiore, G. L., et al. (2011). Optically healable supramolecular polymers. *Nature* 472, 334–337. doi:10.1038/nature09963

Cavallo, G., Metrangolo, P., Milani, R., Pilati, T., Priimagi, A., Resnati, G., et al. (2016). The halogen bond. *Chem. Rev.* 116, 2478–2601. doi:10.1021/acs.chemrev.5b00484

Chen, Y., Kushner, A. M., Williams, G. A., and Guan, Z. (2012). Multiphase design of autonomic self-healing thermoplastic elastomers. *Nat. Chem.* 4, 467–472. doi:10.1038/nchem.1314

Clark, T., Hennemann, M., Murray, J. S., and Politzer, P. (2007). Halogen bonding: The σ-hole. *J. Mol. Model.* 13, 291–296. doi:10.1007/s00894-006-0130-2

Cordier, P., Tournilhac, F., Soulie-Ziakovic, C., and Leibler, L. (2008). Self-healing and thermoreversible rubber from supramolecular assembly. *Nature* 451, 977–980. doi:10.1038/nature06669

Dahlke, J., Kimmig, J., Abend, M., Zechel, S., Vitz, J., Schubert, U. S., et al. (2020). Quantification of the scratch-healing efficiency for novel zwitterionic polymers. *NPG Asia Mat.* 12, 13. doi:10.1038/s41427-019-0190-2

Dahlke, J., Tepper, R., Geitner, R., Zechel, S., Vitz, J., Kampes, R., et al. (2018). A healing ionomer crosslinked by a bis-bidentate halogen bond linker: A route to hard and healable coatings. *Polym. Chem.* 9, 2193–2197. doi:10.1039/c8py00149a

Dahlke, J., Zechel, S., Hager, M. D., and Schubert, U. S. (2018). How to design a self-healing polymer: General concepts of dynamic covalent bonds and their application for intrinsic healable materials. *Adv. Mat. Interfaces* 5, 1800051. doi:10.1002/admi.201800051

Desiraju Gautam, R., Ho, P. S., Kloo, L., Legon Anthony, C., Marquardt, R., Metrangolo, P., et al. (2013). Definition of the halogen bond (IUPAC Recommendations 2013). *Pure Appl. Chem.* 85, 1711–1713. doi:10.1351/pac-rec-12-05-10

Enke, M., Döhler, D., Bode, S., Binder, W. H., Hager, M. D., and Schubert, U. S. (2016). Intrinsic self-healing polymers based on supramolecular interactions: State of the art and future directions. *Adv. Polym. Sci.* 273, 59. doi:10.1007/12_2015_345

Garcia, S. J. (2014). Effect of polymer architecture on the intrinsic self-healing character of polymers. *Eur. Polym. J.* 53, 118–125. doi:10.1016/j.eurpolymj.2014.01.026

Gilday, L. C., Robinson, S. W., Barendt, T. A., Langton, M. J., Mullaney, B. R., and Beer, P. D. (2015). Halogen bonding in supramolecular chemistry. *Chem. Rev.* 115, 7118–7195. doi:10.1021/cr500674c

Hager, M. D., Greil, P., Leyens, C., van der Zwaag, S., and Schubert, U. S. (2010). Self-healing materials. *Adv. Mat.* 22, 5424–5430. doi:10.1002/adma.201003036

Han, C. D., and Jhon, M. S. (1986). Correlations of the first normal stress difference with shear stress and of the storage modulus with loss modulus for homopolymers. *J. Appl. Polym. Sci.* 32, 3809–3840. doi:10.1002/app.1986.070320302

Han, S.-I., Gu, B. H., Nam, K. H., Im, S. J., Kim, S. C., and Im, S. S. (2007). Novel copolyester-based ionomer for a shape-memory biodegradable material. *Polymer* 48, 1830–1834. doi:10.1016/j.polymer.2007.02.040

Hawke, L. G. D., Ahmadi, M., Goldansaz, H., and Ruymbeke, E. v. (2016). Viscoelastic properties of linear associating poly(n-butyl acrylate) chains. *J. Rheol. (N. Y. N. Y).* 60, 297–310. doi:10.1122/1.4942231

Kampes, R., Zechel, S., Hager, M. D., and Schubert, U. S. (2021). Halogen bonding in polymer science: Towards new smart materials. *Chem. Sci.* 12, 9275–9286. doi:10.1039/d1sc02608a

Lange, R. F. M., Van Gurp, M., and Meijer, E. W. (1999). Hydrogen-bonded supramolecular polymer networks. *J. Polym. Sci. A. Polym. Chem.* 37, 3657–3670. doi:10.1002/(sici)1099-0518(19991001)37:19<3657::aid-pola1>3.0.co;2-6

Lewis, C. L., Stewart, K., and Anthamatten, M. (2014). The influence of hydrogen bonding side-groups on viscoelastic behavior of linear and network polymers. *Macromolecules* 47, 729–740. doi:10.1021/ma402368s

Lieffrig, J., Jeannin, O., Frąckowiak, A., Olejniczak, I., Świetlik, R., Dahaoui, S., et al. (2013). Charge-assisted halogen bonding: Donor-acceptor complexes with variable ionicity. *Chem. Eur. J.* 19, 14804–14813. doi:10.1002/chem.201302507

Messina, M. T., Metrangolo, P., Navarrini, W., Radice, S., Resnati, G., and Zerbi, G. (2000). Infrared and Raman analyses of the halogen-bonded non-covalent adducts formed by α, ω-diiodoperfluoroalkanes with DABCO and other electron donors. *J. Mol. Struct.* 524, 87–94. doi:10.1016/s0022-2860(99)00445-7

Meurer, J., Hniopek, J., Dahlke, J., Schmitt, M., Popp, J., Zechel, S., et al. (2021). Novel biobased self-healing ionomers derived from itaconic acid derivates. *Macromol. Rapid Commun.* 42, 2000636. doi:10.1002/marc.202000636

Meurer, J., Kampes, R. H., Bätz, T., Hniopek, J., Kimmig, J., Müschke, O., et al. 2022, submitted. doi:10.1002/adfm.202207313

Mukherjee, A., Tothadi, S., and Desiraju, G. R. (2014). Halogen bonds in crystal engineering: Like hydrogen bonds yet different. *Acc. Chem. Res.* 47, 2514–2524. doi:10.1021/ar5001555

Ogawa, T., Sakamoto, N., Hashimoto, T., Han, C. D., and Baek, D. M. (1996). Effect of volume fraction on the Order–Disorder transition in low molecular weight polystyrene-*block*-polyisoprene copolymers. 2. Order–Disorder transition temperature determined by small-angle X-ray scattering. *Macromolecules* 29, 2113–2123. doi:10.1021/ma951066v

Pancholi, J., and Beer, P. D. (2020). Halogen bonding motifs for anion recognition. *Coord. Chem. Rev.* 416, 213281. doi:10.1016/j.ccr.2020.213281

R Core Team (2021). *R: A language and environment for statistical computing*. Vienna, Austria: R Foundation for Statistical Computing. Available at: https://www.R-project.org/.

Robinson, S. W., Mustoe, C. L., White, N. G., Brown, A., Thompson, A. L., Kennepohl, P., et al. (2015). Evidence for halogen bond covalency in acyclic and interlocked halogen-bonding receptor anion recognition. *J. Am. Chem. Soc.* 137, 499–507. doi:10.1021/ja511648d

Rosokha, S. V., Stern, C. L., and Ritzert, J. T. (2013). Experimental and computational probes of the nature of halogen bonding: Complexes of bromine-containing molecules with bromide anions. *Chem. Eur. J.* 19, 8774–8788. doi:10.1002/chem.201300577

Ryan, C. G., Clayton, E., Griffin, W. L., Sie, S. H., and Cousens, D. R. (1988). SNIP, a statistics-sensitive background treatment for the quantitative analysis of PIXE spectra in geoscience applications. *Nucl. Instrum. Methods Phys. Res. Sect. B Beam Interact. Mater. Atoms* 34, 396–402. doi:10.1016/0168-583x(88)90063-8

Seiffert, S., and Sprakel, J. (2012). Physical chemistry of supramolecular polymer networks. *Chem. Soc. Rev.* 41, 909–930. doi:10.1039/c1cs15191f

Shabbir, A., Javakhishvili, I., Cerveny, S., Hvilsted, S., Skov, A. L., Hassager, O., et al. (2016). Linear viscoelastic and dielectric relaxation response of unentangled UPy-based supramolecular networks. *Macromolecules* 49, 3899–3910. doi:10.1021/acs.macromol.6b00122

Shen, M., Huang, W., Chen, M., Song, B., Zeng, G., and Zhang, Y. (2020). (Micro) plastic crisis: Un-ignorable contribution to global greenhouse gas emissions and climate change. *J. Clean. Prod.* 254, 120138. doi:10.1016/j.jclepro.2020.120138

Socrates, G. (2001). *Infrared and Raman characteristic group frequencies : Tables and charts*. edition. Chichester u.a.: Wiley, 3.

Soman, B., and Evans, C. M. (2021). Effect of precise linker length, bond density, and broad temperature window on the rheological properties of ethylene vitrimers. *Soft Matter* 17, 3569–3577. doi:10.1039/d0sm01544j

Sutar, R. L., and Huber, S. M. (2019). Catalysis of organic reactions through halogen bonding. *ACS Catal.* 9, 9622–9639. doi:10.1021/acscatal.9b02894

Tepper, R., Bode, S., Geitner, R., Jager, M., Gorls, H., Vitz, J., et al. (2017). Polymeric halogen-bond-based donor systems showing self-healing behavior in thin films. *Angew. Chem. Int. Ed.* 56, 4047–4051. doi:10.1002/anie.201610406

Teyssandier, J., Mali, K. S., and De Feyter, S. (2020). Halogen bonding in two-dimensional crystal engineering. *ChemistryOpen* 9, 225–241. doi:10.1002/open.201900337

Vanderkooy, A., and Taylor, M. S. (2015). Solution-phase self-assembly of complementary halogen bonding polymers. *J. Am. Chem. Soc.* 137, 5080–5086. doi:10.1021/jacs.5b00754

Varley, R. J., Shen, S., and van der Zwaag, S. (2010). The effect of cluster plasticisation on the self healing behaviour of ionomers. *Polymer* 51, 679–686. doi:10.1016/j.polymer.2009.12.025

Wang, R., George, J., Potts, S. K., Kremer, M., Dronskowski, R., and Englert, U. (2019). The many flavours of halogen bonds – message from experimental electron density and Raman spectroscopy. *Acta Crystallogr. C Struct. Chem.* 75, 1190–1201. doi:10.1107/s205322961901132x

White, S. R., Sottos, N. R., Geubelle, P. H., Moore, J. S., Kessler, M. R., Sriram, S. R., et al. (2001). Autonomic healing of polymer composites. *Nature* 409, 794–797. doi:10.1038/35057232

Yang, Z., and Han, C. D. (2008). Rheology of miscible polymer blends with hydrogen bonding. *Macromolecules* 41, 2104–2118. doi:10.1021/ma7025385

Zechel, S., Geitner, R., Abend, M., Siegmann, M., Enke, M., Kuhl, N., et al. (2017). Intrinsic self-healing polymers with a high E-modulus based on dynamic reversible urea bonds. *NPG Asia Mat.* 9, e420. doi:10.1038/am.2017.125

Zhang, M., Xu, D., Yan, X., Chen, J., Dong, S., Zheng, B., et al. (2012). Self-healing supramolecular gels formed by crown ether based host-guest interactions. *Angew. Chem. Int. Ed.* 51, 7011–7015. doi:10.1002/anie.201203063